Clim. Past Discuss., 7, 3131–3164, 2011
www.clim-past-discuss.net/7/3131/2011/
doi:10.5194/cpd-7-3131-2011

Climate of the Past Discussions

This discussion paper is/has been under review for the journal Climate of the Past (CP). Please refer to the corresponding final paper in CP if available.

Little ice age advance and retreat of Glaciar Jorge Montt, Chilean Patagonia, recorded in maps, air photographs and dendrochronology

A. Rivera[1,2], M. Koppes[3], C. Bravo[1], and J. C. Aravena[4]

[1]Centro de Estudios Científicos (CECS), Valdivia, Chile
[2]Departamento de Geografía, Universidad de Chile, Santiago, Chile
[3]Department of Geography, University of British Columbia, Vancouver, Canada
[4]Centro de Estudios Cuaternarios de Fuego Patagonia y Antártica (CEQUA), Punta Arenas, Chile

Received: 2 September 2011 – Accepted: 5 September 2011 – Published: 5 October 2011

Correspondence to: A. Rivera (arivera@cecs.cl)

Published by Copernicus Publications on behalf of the European Geosciences Union.

Abstract

Glacier Jorge Montt (48°20′ S/73°30′ W), one of the main tidewater glaciers of the Southern Patagonian Icefield (SPI), has experienced the fastest frontal retreat observed in Patagonia during the past century, with a recession of 19.5 km between 1898 and 2011. This record retreat uncovered trees overridden during the Little Ice Age (LIA) advance of the glacier. Samples of these trees were dated using radiocarbon methods, yielding burial ages between 460 and 250 cal yr BP. The dendrochronology and maps indicate that Glaciar Jorge Montt was at its present position before the beginning of the LIA, in concert with several other glaciers in Southern Patagonia, and reached its maximum advance position between 1650 and 1750 AD. The post-LIA retreat is most likely triggered by climatically induced changes during the 20th century, however, Glaciar Jorge Montt has responded more dramatically than its neighbours. The retreat of Jorge Montt opened a new fjord 19.5 km long, and up to 391 m deep, with a varied bathymetry well correlated with glacier retreat rates, suggesting that dynamic responses of the glacier are at least partially connected to near buoyancy conditions at the ice front, resulting in high calving fluxes, accelerating thinning rates and rapid ice velocities.

1 Introduction

The Patagonian Icefields (Fig. 1) are the largest temperate ice masses in the southern Hemisphere, comprised of two main ice bodies, the Northern and the Southern Icefields (NPI and SPI, respectively), which include 118 inventoried glaciers and a total ice-covered area of approximately 17 000 km^2 (Rivera et al., 2007; Aniya et al., 1996). Most of these glaciers have been retreating steadily since the end of the Little Ice Age (LIA), dated to between 1650 and 1750 AD (Glasser et al., 2010). Despite a general retreating trend since the end of the LIA (Rignot et al., 2003; López et al., 2010), some glaciers, especially Glaciares Moreno, Pío XI and Trinidad in the SPI, have demonstrated anomalous positive behaviour, advancing during the 20th century well after the end of the LIA (Rivera et al., 1999; Masiokas et al., 2009). Others have suffered rapid retreats into deep lakes and fjords, such as Glaciar O'Higgins (Casassa et al., 1997) and Glaciar Upsala (Skvarca et al., 2002). These anomalously rapid retreats have been related to (1) calving characteristics of the ice fronts, (2) ice flow acceleration in the lower reaches of the glaciers, and (3) surface elevation changes as the glaciers thin and shrink. All three factors are ultimately triggered by climate variability and regional warming, however, the specific behaviour of each ice body will depend on other factors, including the bathymetry of the lakes or fjords into which the glaciers are calving, which may influence the volume of ice lost to calving and which may be a cause, or a consequence of, any acceleration in ice flow (Benn et al., 2007).

The western (Chilean) side of Patagonia, where many of the glaciers that calve into seawater are located, is an archipelago with thousands of islands and channels. The region has been visited since the 16th century as numerous explorers crossed the Strait of Magellan (Martinic, 1999). One of the first visitors to leave an account of a perilous trip was Juan Ladrillero, who navigated western Patagonia in 1597/1598. During his explorations, navigation was made challenging by the many icebergs coming from Glaciar Pío XI, at the end of Fiordo Eyre (Bertrand, 1880). This and other narratives of icebergs in historical accounts have been used to define a cold period during the second half of the 16th century (Prieto and Herrera, 1998), coincident with the beginning of the LIA, which reached its maximum extent around 1650 AD (Villalba, 1994; Villalba et al., 2003).

The first effort to map glaciers in Patagonia was conducted by King (1839), using data collected during the British Hydrographic expeditions of 1826–1830 onboard the HMS Beagle, Adventure and Adelaide (which included Charles Darwin, the famous naturalist, among other members of the crew). Between January and April 1830, the HMS Adelaide, under Lieutenant Skyring, mapped Fiordo Eyre, including the ice front position of Glaciar Pío XI. Comparing his map to the present (2011) position of the glacier front, Pío XI has advanced almost 12 km.

Despite these dramatic accounts of Pío XI, very little is known about the long term historical variations of other glaciers in the SPI, such as Glaciar Jorge Montt (48.2° S/73.5° W, 447 km^2 in 2009). Jorge Montt is one of the main tidewater calving glaciers of the SPI, flowing north from one of the central plateaus of the SPI (shared with Glaciares Occidental, Témpano and Bernardo, among others) (Fig. 1). The glacier calves into an unnamed fjord that opened as a consequence of glacier retreat since 1898, when the first map to include the glacier was published by Steffen (1910). At this time, the ice front extended to within 3 km of Fiordo Calen, also known as Canal Baker (Fig. 2). The lower tongue has been thinning dramatically in recent decades, with an areal thinning rate of 3.3 $m\,yr^{-1}$ between 1975 and 2000, the fastest thinning rates observed in Patagonia (Rignot et al., 2003).

In this paper, we present the 20th century changes from Glaciar Jorge Montt. The main purpose of this paper is to understand calving glacier behaviour during and since the LIA, considering local topographic conditions and their possible influence on glacier dynamic responses. We present all available historical records, aerial photographs and satellite imagery of the glacier, which we use to analyse in detail changes in ice front position before and after the Little Ice Age, and compare these changes to a recent survey of the bathymetry of the opening fjord as well as to dendrochronologic dates collected near the 2010 terminus. We then compare these historical variations to changes documented at other glaciers within the northern SPI, in order to highlight the key variables that drive differences in glacier response to regional climate change.

2 Data and methods

2.1 Historical accounts

A first historical account of Glaciar Jorge Montt was recorded at the end of the 16th century. This record left no map, and the description is very difficult to map and interpret. Several historical accounts from the 19th century have been found, due to the Chilean

Boundary Commission, who travelled through southern Chile mapping the region while looking for the continental watershed divide, among other features. These accounts are not very precise, but they contain sufficient detail to fix glacier positions and characterize some of the lower ice tongues.

2.2 Aerial photographs

The oldest aerial photos collected in Patagonia were acquired in 1944/1945 by the United States Air Force, which surveyed the whole of Southern Chile, collecting the first aerial photographs of the region. The TRIMETROGON flight was composed of one vertical and two oblique lines of photographs. The TRIMETROGON aerial survey was used to prepare a 1:250 000 preliminary cartography of Patagonia, including the position of almost every glacier in the Patagonian icefields, but did not include the surface topography of the ice, which was only preliminarily estimated. Subsequent aerial photo surveys only collected vertical images, including the so-called McHurd photo series taken in 1975, at approximately 1:50 000 scale.

The aerial photos collected in Patagonia are available solely as paper copies, and many of the series have no overlapping areas for photogrammetric analysis. The photos were analysed with stereoscopes, and then scanned and adjusted to modern cartography using GIS software, enabling us to geo-reference the scanned photos to the most recent cartography. The errors inherent in using this procedure to adjust the photos to satellite images or cartography is considerable when applied to the whole photo, however, the accuracy improves significantly when focusing on particular areas within the image, such as the ice fronts.

2.3 Satellite images

The oldest available satellite images of the region were collected by the Corona spy satellite in 1963, and by the Keyhole sensor in 1979. In August 1963, the first Corona satellite image of the Patagonian icefields was collected in what is now known as "the

declassified mission" (Table 1). Given the midwinter acquisition date of the imagery, most of the icefields are covered in snow, however, the frontal positions of many of the SPI glaciers are clearly visible, allowing the termini to be mapped accurately. These images are also only available as paper copies, and were analysed using the same procedure as for the aerial photographs, described above.

In 1976, with the launch of the Landsat MSS satellite series, the frequency of images from the SPI increased. In 1976, the first Landsat MSS successfully collected images from the region, and these were made digitally available (Table 1). In 1979, two images are available, one from March and second from August, which show no significant change in glacier position between 1976 and 1979.

The digital satellite images were geo-referenced to regular cartography, and orthorectified using the Space Shuttle Radar Topography mission (SRTM) data set. A manual adjustment was applied to ensure a more precise overlap between the images, using tie points selected from the most clearly visible features around the study area. Considering the resolution of the images and the geo-referencing process, a systematic horizontal error is assumed according to the method described in Williams et al. (1997) and Rivera et al. (2007), where pixel size is multiplied by the perimeter of the changing portion and averaged by the time interval.

The full dataset of satellite images was projected into a Universal Transversal Mercator format (UTM-zones 18S and 19S) under the WGS84 datum. Database management and analysis were carried out using GIS tools from ENVI 4.5 and ArcMap.

Several false-colour composite images derived from the visible and/or near infrared bands were obtained by layer stacking procedures (Paul et al., 2002), including Landsat 5/4/3, Landsat 5/4/1 and ASTER 3/2/1; this produced the best discrimination between the glaciers and non-glaciated surfaces (vegetation, water bodies and seasonal snow patches). Glacier outlines were manually digitised from each image. Ice divides were obtained by overlapping SRTM layers on satellite composite images, and then deriving contour lines from the SRTM DEM, allowing us to define the main glacier flow lines.

A full coverage mosaic of the SPI was acquired in October 2000 with a Landsat ETM+ image (Table 1). This mosaic allowed mapping the basin outlines of the glaciers analysed. These basin outlines are similar to the polygons drawn by Aniya et al. (1996), with minor modifications due to the addition of the SRTM data.

Unfortunately, the only satellite image available for the 1990s was obtained in 1997. Cloud cover in this image is considerable, however, the ice front is distinguishable between the mist and the brash ice covering most of the newly vacated fjord, generated after significant glacier retreat in the prior decade.

Two ASTER scenes were acquired in 16 and 25 February 2010 (Table 1), at the end of the austral summer, and used to estimate the most recent Equilibrium Line Altitudes (ELA) of the major glaciers of the SPI.

2.4 Topographic data

The first detailed topography of the area was based upon the McHurd aerial photographs of 1975, and was prepared by the Military Geographical Institute of Chile (IGM) at 1:50 000 scale. The map includes the ice front position of Glaciar Jorge Montt and the surface topography of the glacier up to approx. 1000 m a.s.l., where the stereoscopic capabilities of the aerial photographs was lost due to white surfaces covered by fresh snow. The spatial resolution of the DEM derived from this map is 50 m and the vertical accuracy is 19 m (Rivera et al., 2007).

In 2000, the region was included in the SRTM DEM dataset. The available resolution of the SRTM data is 90 m for Patagonia, and the glaciers are almost completely included in the DEM except for in the upper reaches of the plateaus, within the accumulation areas, where data was scarce. The vertical accuracy of this dataset is better than 16 m (Bamber and Rivera, 2007). Hypsometric curves of the main glaciers were derived from SRTM data using the glacier basins for the same year (2000).

In December 2002 and 2008, airborne campaigns were conducted from a Chilean Navy Orion P3 airplane using the NASA Airborne Topographic Mapper (ATM) laser to survey the surface topography of Glaciar Jorge Montt. The campaign covered two

longitudinal profiles from sea level up to the ice divide, with decimeter accuracy (Krabill et al., 1995).

The ASTER scene acquired in 16 February 2010 was selected for an ASTER DMO (on demand) DEM, with spatial resolution of 30 m and vertical accuracy of 21 m.

2.5 Bathymetry

In February 2010, we conducted a field campaign to the glacier by boat. Access to the ice front was challenging due to the vast amount of brash ice in the inner fjord, confirming high calving rates of the glacier. In spite of these difficulties, the terminus of the glacier was reached and mapped via zodiac. We also were able to explore the western margin of the glacier, where two stereographic time-lapse cameras were installed in order to measure surface ice velocities (Rivera et al., 2011a). These cameras collected continuous imagery until 22 January 2011.

The depth and subsurface of the new fjord left by the retreating glacier was surveyed with the following instruments/methods: (1) a GARMIN GPS-sonar receiver model GPSMAP 188c, able to locate the position of each bathymetric measurement (3 m accuracy), as well as to penetrate up to 420 m of salty water. This receiver was mounted on a Zodiac gum boat navigating close to the glacier front, trying to avoid the huge amount of brash ice at the inner fjord. (2) A FURUNO sonar system installed on the yacht provided by the private company Waters of Patagonia, which provided logistical support during the February 2010 campaign to the area. (3) A Datasonics Bubble Pulser sub-bottom profiler, using a 4 m long hydrophone and GeoAcoustic amplifier. This system allowed us to survey deeper waters, as well as map the submarine sediments in the fjord. It was able to penetrate up to 250 m of soft sediment deposits. The analysis of these sediments is part of a subsequent study.

More than 26 000 bathymetric datapoints were collected in the fjord in February 2010. The data were collected along longitudinal and traverse tracks crossing the fjord at approx. 500 m spacing. The data coverage was very dense in some parts of the fjord, whereas other regions were sparsely surveyed due to the presence of brash ice and icebergs precluding navigation. The area near the ice front in February 2010 was surveyed along a transverse profile located only 100 m from the terminus ice cliff. Using all available data points, a linear interpolation method was applied to infer the bathymetry between tracklines, resulting in a bathymetric map of the fjord with 20 m contour intervals.

2.6 Dendrochronology

In February 2010, whilst surveying the glacier margin, several pieces of semi-buried *Nothofagus sp.* trees were discovered in a small, lateral valley only 250 m from the glacier margin. From the outermost perimeter of these trees, samples were collected for radiocarbon analysis. Samples were sent to the Beta Analytic Radiocarbon Dating Laboratory for ^{14}C dating. The INTCal04 database was used for radiocarbon age calibration, following the approach of Talma and Vogel (1993).

In January 2011, thirteen cross sections were obtained from the same *Nothofagus sp.* trees discovered close to the glacier margin in February 2010. The sections were analyzed following standard dendrochronological procedures and 26 radii were measured and cross-dated to construct a floating (i.e. without calendar ages) tree-ring chronology of the region.

3 Results

3.1 Historical extent of Glacier Jorge Montt

The first detailed account of this glacier was written by Dr. Hans Steffen, an expert German geographer, hired by the Chilean Boundary Commission to study the geography of Patagonia in preparation for the Chilean position at the arbitration tribunal dealing with the boundary controversy between Chile and Argentina (Pozo, 2005). He visited the area in December 1898 onboard the steamer Condor, mapping the area (Fig. 2).

During this trip, he spotted a great glacier (Ventisquero in Spanish), covered in long lateral and medial moraines, descending from the icefield located to the south and calving into Fiordo Baker (Steffen, 1898). This glacier was later named Jorge Montt in honour of a president of Chile (1891–1896). A decade later, Risopatrón (1910), also working for the Chilean Boundary Commission, published a more comprehensive map of the whole region, confirming that the terminus of Glaciar Jorge Montt was in a similar position to that of the Steffen survey of 1898.

In 1944/1945, the United States Air Force surveyed Southern Chile, collecting the first aerial photographs of the region. Thanks to this survey, the terminus position of Glaciar Jorge Montt was ascertained, confirming it had retreated approximately 6.7 km since 1898, yielding a retreat rate of 146 m yr^{-1} (Table 2). The photos also confirmed the presence of the moraine bands described by Steffen (1898), but by this time only the lateral moraine on the eastern side of the tongue reached directly into the ocean, while the lateral moraine on the western side had a more complex shape consisting of two lateral flows, not reaching the ocean but terminating in a side valley where both flows joined together and were partially calving into a small freshwater lagoon.

In the 1963 Corona image, Glacier Jorge Montt is visible at the northern side of the SPI reflecting a moderate frontal retreat of 195 m since 1945 (Table 2). The lower tongue of the glacier is partially debris covered, especially the western margin which ends in a lateral valley, as seen in the 1945 photo. In 1963, both lateral moraines of Jorge Montt are reaching the ocean, and little ice is visible in the western side valley described in 1945 as partially occupied by ice with a complex surface moraine shape. In the region where in 1945 the left lateral arm was overflowing into the lateral valley, by 1975 a small tongue has deviated from the main ice flow direction, and protrudes 2 km into this lateral valley, ending in a steep slope without any visible calving activity. The now ice-free western valley shows a river coming from the upper slopes, a marshy area and a lake. The whole valley is covered by grass and is free of forest cover, indicating that the ice covering this area had melted away in situ (dead ice) at some time since 1963. Between 1976 and 1963, the ice front retreated 530 m (Table 2).

Discussion Paper | Discussion Paper | Discussion Paper | Discussion Paper |

The glacier in 1976 is calving into the fjord, with both lateral moraines reaching sea water. No dead ice is visible in the western lateral valley. Between 1976 and 1979 the central part of the glacier in the middle of the fjord retreated 321 m, whilst the western margin remained relatively stable (Fig. 3).

During the 1980s the glacier front was quite stable, with minor fluctuations and minimum retreats, however around 1990 the glacier underwent a sudden, dramatic and almost catastrophic retreat, with the glacier retreating 8 km in a decade. Interestingly, in the 1997 image, the western side of the calving front extends 3 km north in a narrow lateral band along the fjord edge. This partially debris-covered ice is a remnant portion of the retreating glacier, hanging onto the margin of the fjord as grounded ice, with little calving activity. This type of "dead ice", almost disconnected from the main trunk of the glacier and therefore not fed by new ice coming from the upper reaches of the icefield, is melting in situ, with a small amount of calving along the margin in contact with the fjord water.

After undergoing significant retreat in the 1990s, the glacier front stabilized and retreat slowed during the 2000s. The "dead ice" observed in the 1997 image is gone and the lateral moraines are calving directly into the fjord. However, by 2000, a new area of debris covered "dead ice" was observed extending 1.5 km north of the 2000 calving front along the western margin of the glacier, with a similar narrow shape compared to that observed in 1997. This region of stagnant ice, almost detached from the main glacier, was free of ice by 2003, when the entire glacier front calved directly into the fjord without lateral extensions along the margins. Due to the disappearance of the stagnant ice, several trees that had been buried in-situ were uncovered, which were sampled for ^{14}C dating in February 2010 (see location of samples in Fig. 3).

The time-lapse imagery collected in 2010–2011 shows a further retreat of the terminus of ~1 km, with a total area lost yielded 1.48 km^2 during 2010. The images also captured a massive calving event over the course of 9 days, from 16–25 February 2010 with a total area lost of 0.31 km^2. Analysing the photos closely, many calving events were observed to produce large icebergs, some with semi tabular shapes.

The fjord remained predominantly covered by icebergs and brash ice throughout the year, however, the front of the glacier also showed evidence of upwelling, as seen in semi-circular, ice-free areas of open sea water next to the ice front. Along both lateral margins of the main tongue, narrows bands of debris-covered ice were hanging from the mountain flanks. These "dead ice" areas were almost disconnected from the main glacier flow and melting in situ.

3.2 Bathymetric survey

The area surrounding the 1898 position of the glacier (Figs. 4 and 5) indicates that the bathymetry around this stable advance position was coincident with a submarine moraine arc crossing the fjord with minimum water depths of 16 m and a narrow channel of ~45 m depth along the western edge of the outer fjord.

The main channel of the outer fjord, between the 1898 and 1945 terminus positions (Fig. 4) is typically "U" shaped with a flat bottom of maximum depth 115 m. The 1945 terminus coincides with another subaqauatic ridge of less than 80 m water depth.

The area between the 1945 and 1990 terminus positions shows a gently sloping bathymetry of increasing water depth. Between the 1990 and 1997 ice front positions, the fjord bottom drops steeply to reach a maximum depth of 370 m (Fig. 4). This deep part of the fjord coincides with the timing of the most rapid retreat during the 1990s. It also coincides with the period when the glacier underwent the strongest thinning.

Further upfjord of the 1997 terminus position, water depths decrease to a mean of −210 m close to the ice front in 2000–2003, before dropping again to a maximum depth of −391 m at the 2010 ice front (Fig. 6).

3.3 Thinning rates

The surface topography of the glacier during the latter half of the 20th century changed dramatically. The 1975 topography, compared to the SRTM topography (2000), was

Discussion Paper | Discussion Paper | Discussion Paper | Discussion Paper |

analysed by Rignot et al. (2003), yielding a maximum thinning rate of 18 m yr^{-1} between 1975 and 2000.

Between 2000 and 2002 (Fig. 6), comparing the LIDAR profiles measured during the airborne P3 campaign, the glacier thinned at a mean rate of 31 m yr^{-1}, the maximum rate of thinning recorded for this glacier. Between 2002 and 2008, the same LIDAR profiles resulted in a mean thinning rate of 2.8 m yr^{-1}, then increased again between 2008 and 2010 to 22 m yr^{-1}.

3.4 Ice velocities

The first measurements of ice velocity at Jorge Montt were collected by Enomoto and Abe (1983), who measured surface velocities of 240 m yr^{-1} at the terminus. Using speckle tracking from RADARSAT-1 images collected in 2004, Eric Rignot (personal communication, 2011) obtained values of up to 3460 m yr^{-1}, at a location 3 km upstream the glacier front. More recently, based upon feature tracking of geo-referenced photos from the fixed cameras installed in 2010, Rivera et al. (2011) obtained a mean value of 4885 m yr^{-1} for a complete transverse cross-section at the glacier front, indicating significant acceleration of ice flow in the past three decades (Rivera et al., 2011a).

3.5 Tree samples

The first sample (Fig. 7), located along the margin of a proglacial stream 250 m from the 2010 glacier margin, was dated to 460 ± 40 ^{14}C BP, with a calibrated age of 1440 cal AD. The second sample, collected approximately 50 m from sample 1, was dated to 250 ± 40 BP, with a calibrated age of 1650 cal AD. The almost 200 year difference in age between the samples must reflect timing of death of the trees and not differences in burial dates or separate glacial advances, as both samples were collected from the same subglacial deposit, in close proximity, and were both partly buried in the same thin layer of till. The area was scoured by the glacier and most of

the surface was bare rock with lag boulders, hence there is very little evidence of significant sediment reworking that would reset ages and reflect multiple glacial advances in the area.

Sixteen out of the 29 measured radii were successfully cross-dated with a mean correlation of 0.457. The resulting floating chronology covers 276 years, with high interannual variability (Fig. 8).

The tree-ring results suggests the area was covered in an old-growth forest dominated by *Nothofagus betuloides* ("coigue de Magallanes" – Magellanic southern beech) with individuals of average age close to 150 years, co-existing for almost 300 years (total chronology length). The radiocarbon ages of between 250 and 450 yr BP from two of the sampled trees suggests that the tree ring samples were taken from a mature forest that was destroyed by the advance of Glaciar Jorge Montt during the LIA.

4 Discussion

The change in the glacier retreat rate is well correlated to the bathymetry (Fig. 9), with retreat rates increasing with increasing water depths, as postulated by calving theory (e.g. Meier and Post, 1987; Benn et al., 2007). The relationship, however, is not linear, but suggests a polynomial fit ($r^2 = 0.67$). The fastest retreat occurred in the 1990s and again in the past two years, when the fjord bottom exceeded −350 m. This also coincides with the timing of the most rapid ice acceleration and thinning, and suggests that calving is increasing with both water depths as well as with higher ice velocities and more rapid thinning, leading to losses at the ice front in excess of ice flux to the terminus.

In order to better understand the relationship between the bathymetry and changes in glacier extent, we also investigated the calving flux. To first order, calving flux can be calculated from the fjord cross-sectional bathymetry, the retreat rate and ice velocities, where known (Skvarca et al., 2002). Unfortunately, measured ice velocities are very scarce in Patagonia, and only three measurements are available at Jorge Montt, albeit showing steady acceleration in recent decades.

Using the mean glacier frontal calving velocities based on the depth averaged ice velocity plus the frontal change for each period (7.3 m d^{-1} in 2004 and 13.3 m d^{-1} in 2010), the fjord cross-sectional bathymetry (area of 0.26 km^2 in 2004 and 0.32 km^2 in 2010), calving fluxes were 0.72 km^3 yr^{-1} in 2004 and 2.4 km^3 yr^{-1} in 2010. These values are indicating calving acceleration and are higher than previous estimations obtained in Patagonian glaciers (Warren and Aniya, 1999). The question remains, however, as to whether these calving losses are the cause or the consequence of flow acceleration. A concerted modelling approach is needed to answer this question, which is beyond the scope of this study.

The dates of the radiocarbon samples collected at Jorge Montt are coincident with previous dendrochronologic samples obtained by Mercer (1970) at Glaciares Bernardo and Témpano (Fig. 1). Glaciar Bernardo (48°37′ S, 73°54′ W, 527 km^2 in 2009) currently calves into a lake which formed in 1986 when the terminus retreated 2 km from an outwash plain surrounded by its LIA moraine, dated by Mercer to 270 ± 90 yr BP (Mercer, 1970). The terminus was grounded on the outwash plain in 1945, seen in the US Air Force aerial photos. Mercer estimated that Glaciar Bernardo reached its maximum extent around 1775 AD, only a couple of hundred meters downstream from its 1945 position. Glaciar Témpano (48°43′ S, 73°58′ W, 304 km^2 in 2009), is another tidewater glacier where Mercer (1970) observed four distinct lateral moraines that formed in the past few centuries, most likely around 1760 AD, the maximum advance of the LIA. The LIA advance of Glaciar Témpano is also very close to its terminus position in 1945; the terminus has since retreated 4.5 km to its present position. Given these dates, these nearby glaciers experienced a simultaneous advance during the LIA, however the magnitudes of the LIA advances were significantly different. Glaciar Jorge Montt has retreated 19.5 km since the LIA, whereas Bernardo retreated only 2 km and Témpano 4.5 km. Differences in calving characteristics could be one contributor to these differences in terminus behaviour, however, Glaciar Témpano is a tidewater calving glacier much like Jorge Montt.

Another difference between these glaciers are their hypsometries, or area-altitude distributions (Rivera et al., 2011b). The hypsometries of Glaciares Jorge Montt and Témpano are very similar, with a large accumulation area situated on a broad plateau surrounded by peaks, and a narrow tongue gently flowing down an outlet valley. In contrast, Bernardo has a much steeper accumulation area and a smaller ablation area. Based upon the February 2010 ASTER image, the ELA for all three glaciers was estimated to be approximately 1100 m a.s.l.; the resulting accumulation area ratios (AAR) approach 0.62 for Jorge Montt, 0.58 for Témpano and 0.81 for Bernardo.

With a gentle slope at the elevation of the ELA, the mass balance of Jorge Montt is much more sensitive to shifts in the ELA, especially when the ELA intersects the broad accumulation plateau. For a similar rise in ELA, the steeper topography of Bernardo means that changes in mass balance will be smaller, i.e. the glacier is less sensitive to climatic change. This condition, and the smaller AAR, partially explains why Jorge Montt and Témpano have retreated more dramatically than Bernardo in the past few decades. Given continued warming in the region, however, a further rise in the ELA at Bernardo may cause the ELA to intersect its flatter upper accumulation area, possibly triggering an accelerated reduction of its AAR and resulting in frontal retreat rates more similar to that seen at its neighbours.

Another interesting characteristic of Glaciar Jorge Montt is the presence of dead, or stagnant, ice along the margins of the retreating tongue. The topography surrounding the main glacier tongue is flat enough to detach some of the ice from the main flow of the glacier. For example, in 1945, the lower part of the glacier flowed over a low ridge on the western flank of the glacier and occupied a lateral valley, where the ice melted in situ, with only a small portion of the ice front calving into a proglacial lagoon. The same conditions were observed in 1963, 1997, 2000 and most recently in the time-lapse photos collected between 2010 and 2011. The importance of this "dead ice" is that it can act to preserve subglacial and organic material overridden by the ice, such as the buried trees found in 2010. As the ice along these margins is not flowing very fast if at all, subglacial deposition and minimal abrasion can preserve the pre-glacial landscape. These locations are therefore promising sites for more detailed investigations of material overridden by glacial advance during the LIA, which are likely well preserved. The stagnant ice also confirms the importance of calving in driving retreat of the ice front, since the ice that grounded above sea level remained in place for years after the main tongue that reached sea level (and below) had retreated.

The water depth at the end of the new fjord (2010 glacier position), has a maximum of −391 m, implying a near buoyancy condition for the frontal portion of the ice tongue. The height above buoyancy, or ice thickness in excess of flotation (F), is defined as

$$F = (h + w) - w\, s\rho / i\rho \tag{1}$$

Where w is the water depth near the 2010 ice front, h is the mean ice height above water level near the front, $i\rho$ is the ice density (900 kg m^{-3}), and $s\rho$ is the density of sea water (1024 kg m^{-3}). Given $w = 391$ m and $h = 75$ m in 2010, F yields 21 m, a value very close to the ice cliff height of the glacier. Analysing the sequence of time-lapse images obtained with the fixed cameras, the ice front terminates in a clear, prominent and tall cliff with heights that fluctuated between 0 and 45 m a.s.l. in 2010, with a mean of 22 m a.s.l. In many of the images, a large number of icebergs can be seen calving off the front, several of which were tabular in shape. During the days in which tabular icebergs were generated, the height of the ice cliff is less than 20 m, hence the ice was near floating conditions. When flotation conditions occur, retreat is much more rapid than during periods when the front is grounded.

5 Conclusions

Glaciar Jorge Montt has experienced the fastest rates of retreat observed in Patagonia during historical times and one of the fastest rates of calving in recent decades. While the glacier's variations during and since the Little Ice Age are not unique for the Patagonian Icefields, the level of detail in documenting its response to LIA cooling, and the magnitude of the changes in glacier extent observed, is. Jorge Montt is one of the few glacier basins for which regular data of glacier extent is available, allowing for a detailed monitoring of its fluctuations in the last 112 years (December 1898 to January 2011). This record of ice front fluctuations, combined with a bathymetric survey of the glacier-abandoned fjord, suggests that water depth is a key factor explaining the variability and magnitude of retreat over the past century. The deepest waters in the fjord correlate well with maximum retreat rates, indicating that the ice was at/or very close to buoyancy conditions throughout much of the past few decades; a condition that can be catastrophic for a temperate calving glacier like Jorge Montt. Near buoyancy conditions were observed in the time-lapse imagery collected from the ice front in 2010, where tabular icebergs were observed calving from the terminus, suggesting that large portions of the front were at or near flotation. Rapid calving into deeper water clearly drove catastrophic retreat during the 1990s, and again from 2009 to 2011 when the front reached the deepest part of the fjord (−391 m b.s.l.). In contrast, the glacier was stable when its front was grounded on an underwater moraine arc in the outer fjord coincident with the 1898 position of the glacier, and again in 1945 when it grounded on a submarine ridge separating the outer from the inner fjord.

Radiocarbon dating of samples collected near the present glacier front, indicates that the glacier front had retracted to its current 2011 position just before the start of the Little Ice Age. During the LIA advance, a proglacial forest was overridden and remained buried and preserved throughout the LIA, and re-appeared in 2003 when the ice covering the dead trees retreated. During the LIA the glacier advanced to most likely stabilize at the 1898 position, as the terminus location in 1898 is coincident

Discussion Paper | Discussion Paper | Discussion Paper | Discussion Paper |

with a well preserved submerged arcuate moraine, typically generated when the ice advances, removes and reworks subglacial deposits to accumulate in an arcuate form at the maximum stable, advance position.

At least one of buried trees found at Jorge Montt, close to the ice front in 2010, is of similar age to that of tree samples collected near the 1945 positions of Glaciares Bernardo and Témpano, ∼50 km to the southwest. As such, the timing of the start of the LIA advance was simultaneous in at least this part of the SPI. However, the question remains as to why these glaciers exhibited significant differences in the magnitude of their LIA advances: both Bernardo and Témpano were very close to their LIA maxima in 1945 and have only retreated 2–5 km since, whereas Jorge Montt advanced and retreated approximately 19 km north of its LIA maximum. Perhaps the main cause of this difference in LIA extent and subsequent retreat is in the calving dynamics of each of these glaciers, which for Jorge Montt may be influenced by near-flotation conditions in the deep pro-glacial fjord. Another possible cause of differences in glacier length changes could be related to the hypsometries of these glaciers, which is much flatter at the present location of the ELA for Jorge Montt and Témpano than for Bernardo, suggesting that Jorge Montt is much more sensitive to ELA shifts compared to neighbouring glaciers with steeper hypsometries at the present ELA. These significant differences in response to Little Ice Age cooling for nearby and relatively similar glaciers in Patagonia highlight the importance of glacier shapes and ice front dynamics in controlling ice mass responses to regional changes in climate.

Acknowledgements. This research was funded by Fondecyt 1080320. We thank J. C. and Allen Szydlowski (Waters of Patagonia) for providing fantastic logistical support in the field. Bernard Hallet, Chuck Nittrouer, Katie Boldt and Adam Barker from University of Washington, USA, Dick Sylwester, Golder Associates Inc., David Farías, Camilo Rada and Sebastián Cisternas from CECS, Claudia Mansilla and Carla Henríquez from CEQUA, collaborated with this research. The University of Washington participation was rendered possible by funding from the Quaternary Research Center. Satellite images were provided by GLIMS. Andrés Rivera also thanks the Guggenheim Foundation. Thanks to Eric Rignot who provided ice velocity

data. NASA-Wallops provided ATM data. The Chilean Navy provided the Orion P3 for surveying the glaciers in 2002 and 2008.

PAGES PAST GLOBAL CHANGES

The publication of this article was sponsored by PAGES.

References

Aniya, M., Sato, H., Naruse, R., Skvarca, P., and Casassa, G.: The use of satellite and airborne imagery to inventory outlet glaciers of the Southern Patagonia Icefield, South America, Photogramm. Eng. Remote S., 62, 1361–1369, 1996.

Bamber, J. and Rivera, A.: A review of remote sensing methods for glacier mass balance determination, Global Planet. Change, 59, 138–148, 2007.

Benn, D., Warren, C., and Mottram, R.: Calving processes and the dynamics of calving glaciers, Earth Sci. Rev., 82, 143–179, 2007.

Bertrand, A.: Espedición de Juan Ladrillero (1557 a 1559), Anuario hidrográfico de la Marina de Chile, 6, 453–525, 1880.

Casassa, G., Brecher, H., Rivera, A., and Aniya, M.: A Century-long Record of Glaciar O'Higgins, Chilean, Patagonia, Ann. Glaciol., 24, 106–110, 1997.

Cuffey, K. and Paterson, W.: The Physics of Glaciers, 4th Edn., Academic Press, 693 pp., 2010.

Enomoto, H. and Abe, Y.: Reconnaissance Studies of meteorology and glaciology in Steffen and Jorge Montt Glaciers Patagonia, in: Glaciological and Meteorological Studies in Patagonia Chile by Japanese Research Expeditions in 1967–1982, edited by: Naruse, R., Data centre for glacier research, Japanese Society of Snow and Ice, 11–14, 1983.

Glasser, N., Harrison, S., Jansson, K., Anderson, K., and Cowley, A.: Global sea-level contribution from the Patagonian Icefields since the Little Ice Age maximum, Nat. Geosci., 4, 203–207, 2011.

King, P.: Narrative of the surveying voyages of His Majesty's Ships Adventure and Beagle between the years 1826 and 1836, describing their examination of the southern shores of South America, and the Beagle's circumnavigation of the globe, Proceedings of the first expedition, 1826–30, London, 1839.

Krabill, W., Thomas, R., Jezek, K., Kuivinen, K., and Manizade, S.: Greenland ice-sheet thickness changes measured by laser altimetry, Geophys. Res. Lett., 22, 2341–2344, 1995.

López, P., Chevallier, P., Favier, V., Pouyaud, B., Ordenes, F., and Oerlemans, J.: A regional view of fluctuations in glacier length in southern South America, Global Planet. Change, 71, 85–108, 2010.

Masiokas, M., Rivera, A., Espizúa, L., Villalba, R., Delgado, S., and Aravena, J. C.: Glacier fluctuations in extratropical South America during the past 1000 years, Palaeogeogr. Palaeocl., 281, 242–268, 2009.

Meier, M. and Post, A.: Fast Tidewater Glaciers, J. Geophys. Res., 92, 9051–9058, 1987.

Mercer, J. H.: Variations of some Patagonian glaciers since the Late-Glacial: II, Am. J. Sci., 269, 1–25, 1970.

Naruse, R. and Skvarca, P.: Dynamic features of thinning and retreating Glacia Upsala, a lacustrine Calving Glacier in Southern Patagonia, Arct. Antarct. Alp. Res., 32, 485–491, 2000.

Paul, F., Kääb, A., Maisch, M., Kellenberger, T., and Haeberli, W.: The new remote sensing derived Swiss glacier inventory I: Methods, Ann. Glaciol., 34, 355–362, 2002.

Pozo, J.: Hans Steffen: Maestro, Geógrafo y Pionero de la Patagonia Occidental Revista Universum, 20, 112–123, 2005.

Prieto, M. and Herrera, R.: Naos, clima y glaciares en el Estrecho de Magallanes durante el siglo XVI. Anuario de Estudios Americanos, 55, 413–439, 1998.

Rignot, E., Rivera, A., and Casassa, G.: Contribution of the Patagonia icefields of South America to global sea level rise, Science, 302, 434–437, 2003.

Rivera, A., Aravena, J. C., and Casassa, G.: Recent Fluctuations of Glaciar Pío XI, Patagonia: Discussion of a Glacial Surge Hypothesis, Mountain Res. Dev., 17, 309–322, 1997a.

Rivera, A., Lange, H., Aravena, J. C., and Casassa, G.: The 20th Century Advance of Glaciar Pío XI, Southern Patagonia Icefield, Ann. Glaciol., 24, 66–71, 1997b.

Rivera, A., Benham, T., Casassa, G., Bamber, J., and Dowdeswell, J.: Ice elevation and areal changes of glaciers from the Northern Patagonia Icefield, Chile, Global Planet. Change, 59, 126–137, 2007.

Rivera, A., Corripio, J., Bown, F., Rada, C., and Bravo, C.: Patagonian tidewater calving glacier dynamics derived from a full year movie obtained by a fix camera. In: Interactions of Ice Sheets and Glaciers with the Ocean symposium, SCRIPPS, San Diego, USA, Abstract 60A152, 2011a.

Rivera, A., Cawkwell, F., Rada, C., and Bravo, C.: Hypsometry, in: Encyclopedia of Snow Ice and Glaciers, edited by: Singh, V., Singh, P., and Haritashaya, U., Springer, The Netherlands, pp. 551-554, 2011b.

Skvarca, P., De Angelis, H., Naruse, R., Warren, C., and Aniya, M.: Calving rates in fresh water: new data from southern Patagonia, Ann. Glaciol., 34, 379–384, 2002.

Steffen, H.: Informe preliminar sobre los trabajos de la Comisión exploradora del Canal i Rio Baker, ejecutados en la zona del litoral patagónico, comprendida entre los 46° y 48° de latitud sur (diciembre de 1898), in: La Cordillera de los Andes entre las latitudes 46° i 50° S, edited by: Risopatrón, L., 1905, Imprenta Cervantes, Santiago, 113–145, 1898.

Steffen, H.: Viajes de exploración i estudio en la Patagonia occidental 1892–1902, Anales de la Universidad de Chile, Tomo 1 and 2, 549 pp., 1910.

Stuefer, M., Rott, H., and Skvarca, P.: Glaciar Perito Moreno, Patagonia: Climate sensitivities and glacier characteristics preceding the 2003/2004 and 2005/2006 damming events, J. Glaciol., 53, 1–13, 2007.

Talma, A. and Vogel, J.: A Simplified Approach to Calibrating C14 Dates, Radiocarbon, 35, 317–322, 1993.

Villalba, R.: Tree-Rings and glacial evidence for the Medieval Warm Epoch and the Little Ice Age in Southern South America, Climatic Change, 26, 183–197, 1994.

Villalba, R., Lara, A., Boninsegna, J. A., Masiokas, M., Delgado, S., Aravena, J. C., Roig, F. A., Schmelter, A., Wolodarsky, A., and Ripalta, A.: Large-scale temperature changes across the southern Andes: 20th-century variations in the context of the past 400 years, Climatic Change, 59, 177–232, 2003.

Warren, C. and Aniya, M.: The calving glaciers of southern South America, Global Planet. Change, 22, 59–77, 1999.

Table 1. Data used to calculate frontal variations of Jorge Montt Glacier, 1898–2011.

Date (month/day/age)	Sensor	Vertical Spatial Resolution (m)
18 Dec 1898	Historical record (Steffen 1898)	Not applicable
Summer 1944/1945	TRIMETROGON aerial photographs	Oblique
26 Aug 1963	Declassified Corona satellite image	Not available
Summer 1974/1975	Mc Hurd aerial photographs	Not available
25 Feb 1976	Landsat MSS	79
8 Mar 1979	Landsat MSS	79
20 Mar 1979	Keyhole KH-9	Not available
26 Dec 1984	Landsat TM	30
4 Oct 1986	Landsat TM	30
Summer 1990	Landsat TM	30
4 Feb 1997	Landsat TM	30
27 Oct 2000	Landsat ETM+	30
2 Apr 2003	Landsat ETM+	30
4 Feb 2008	ASTER	15
5 Jun 2009	ASTER	15
25 Feb 2010	ASTER	15
15 Jan 2011	Terrestrial photography	Not applicable

Table 2. Frontal variations and water depths along the centreline of the Jorge Montt new fjord.

Period	Number of years (m)	Frontal retreat ($m\,yr^{-1}$)	Frontal change rate (m)	Mean water depth (m)	Maximum water depth (m)
1898–1945	46	6731	−146	−67	−115
1945–1963	18	195	−11	−115	−140
1963–1976	13	530	−41	−140	−168
1976–1979	3	321	−107	−130	−175
1979–1984	5	562	−112	−150	−221
1984–1986	2	41	−20	−220	−228
1986–1990	4	240	−60	−200	−240
1990–1997	7	6600	−943	−220	−370
1997–2000	3	1828	−609	−310	−342
2000–2003	3	422	−141	−210	−279
2003–2008	5	570	−114	−150	−220
2008–2009	1.3	400	−308	−220	−332
2009–2010	0.7	403	−576	−290	−391
2010–2011	0.9	644	−716	Not available	Not available

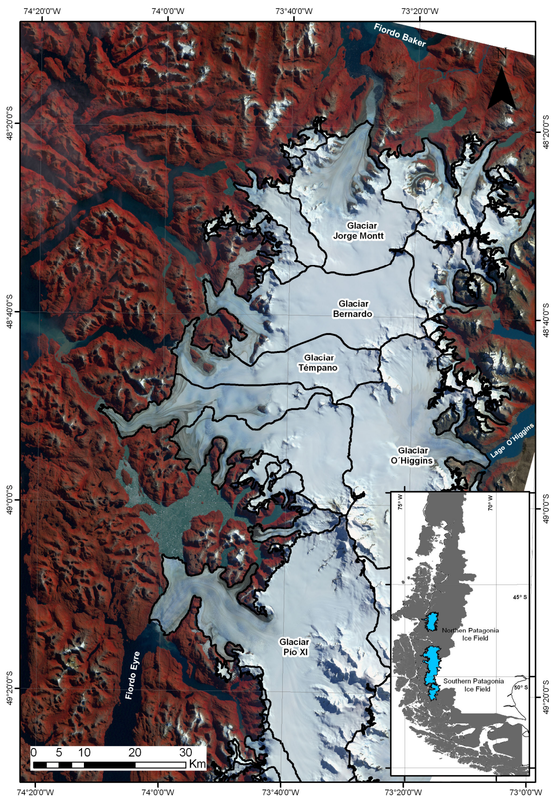

Fig. 1. The main glacier basins of the northern part of the SPI. The background satellite image was acquired on 2 April 2003.

Discussion Paper | Discussion Paper | Discussion Paper | Discussion Paper |

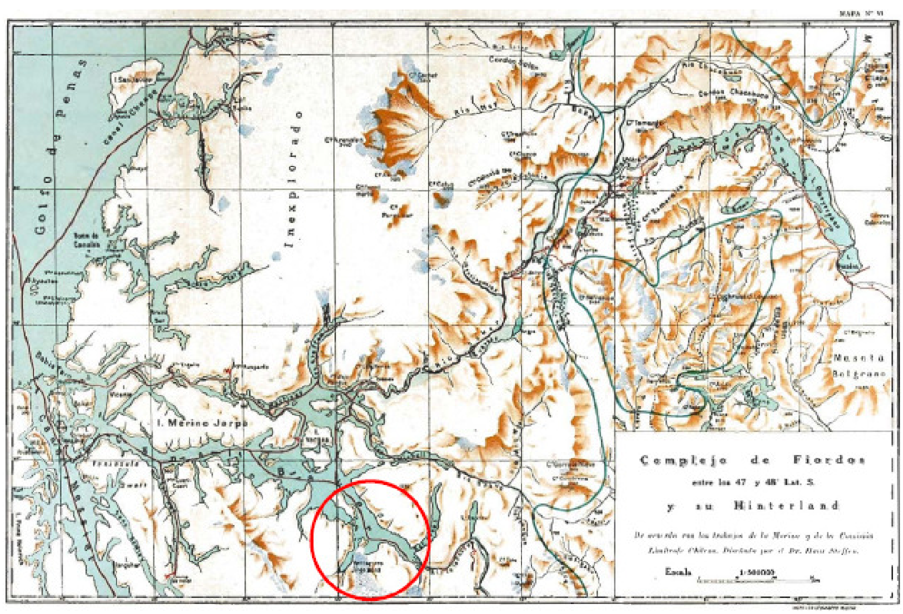

Fig. 2. First map of the northern edge of the SPI as drawn by Steffen in 1898 and published by Steffen (1910). The frontal position of Glaciar Jorge Montt, ~4 km from Canal Baker, is indicated by the red circle.

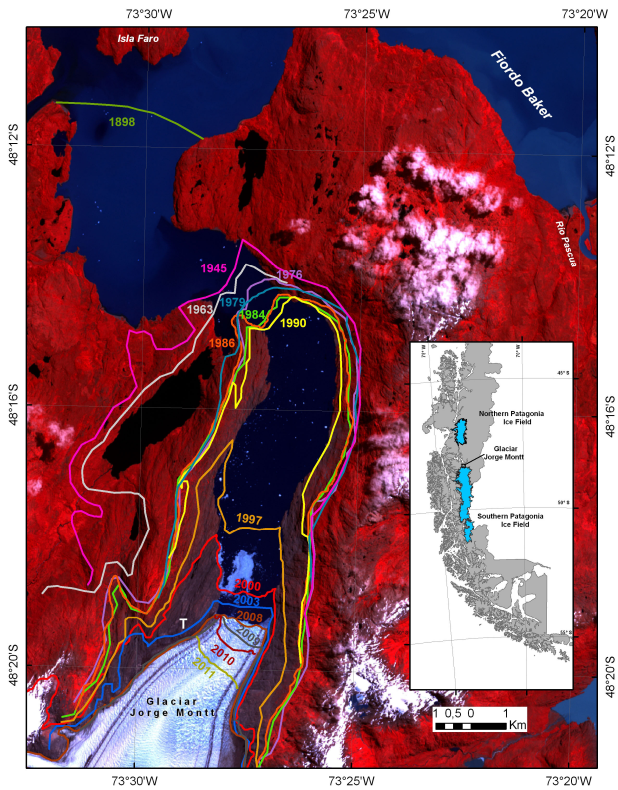

Fig. 3. Frontal positions of Glaciar Jorge Montt, 1898–2011. The location of the dendrochronology sampling sites are indicated to the west of the 2010 terminus (Letter T).

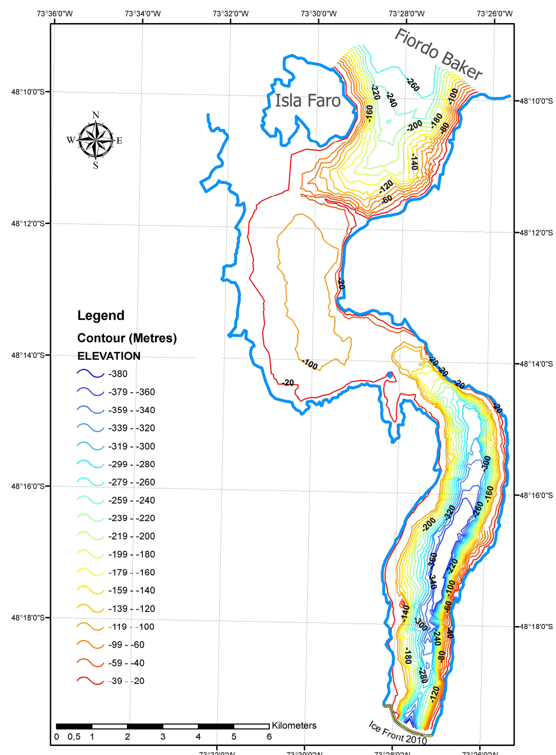

Fig. 4. Bathymetric contour lines from the January 2010 glacier front north to Fiordo Baker (Canal Baker). The glacier front at the end of the Little Ice Age, in 1898, was located near the junction with Fiordo Baker, 1 km south of Isla Faro, where the bathymetry shows a shallow transverse ridge approximately 20 m below sea level.

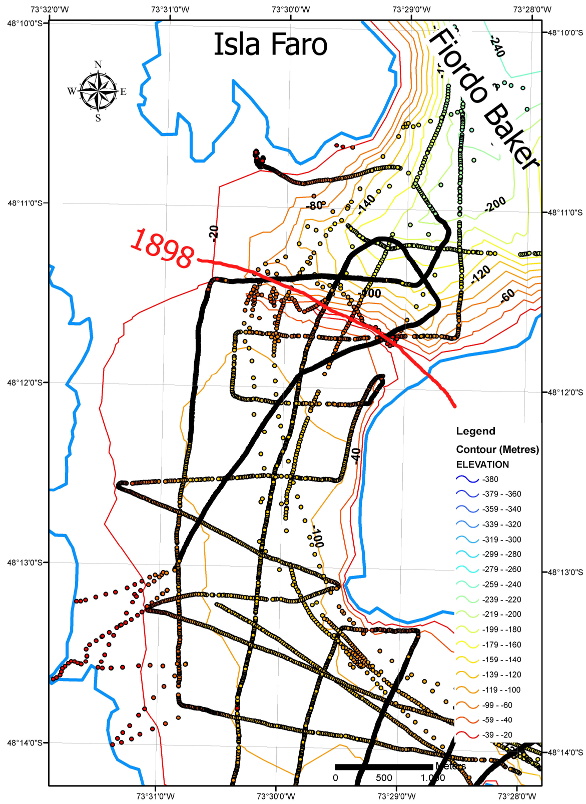

Fig. 5. Data points and interpolated contour lines used to determine bathymetry in the outer fjord, near the 1898 ice front.

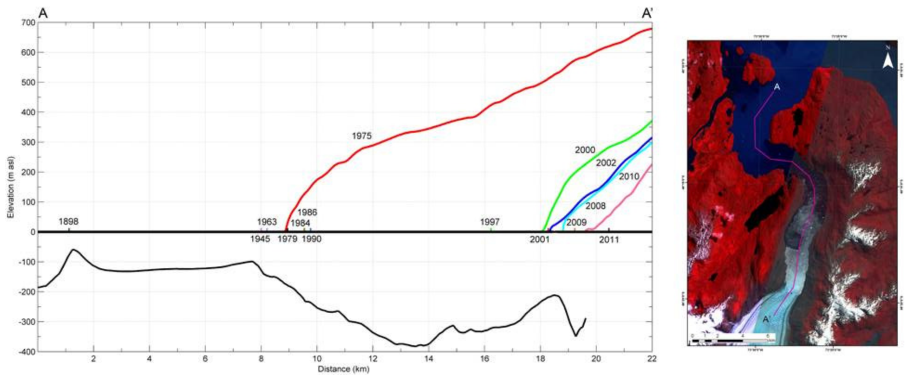

Fig. 6. Longitudinal profile A–A′ along the main axis of the fjord, including the frontal positions of the glacier, the glacier surface topography (coloured lines) and the bathymetry (black line). The inset satellite image (February 2010) shows the location of profile A–A′.

Fig. 7. The buried trees were found near the glacier front in February 2010. In January 2011, cross sections were obtained from these trees. The left side of the image shows brash ice covering the fjord surface waters near the glacier front.

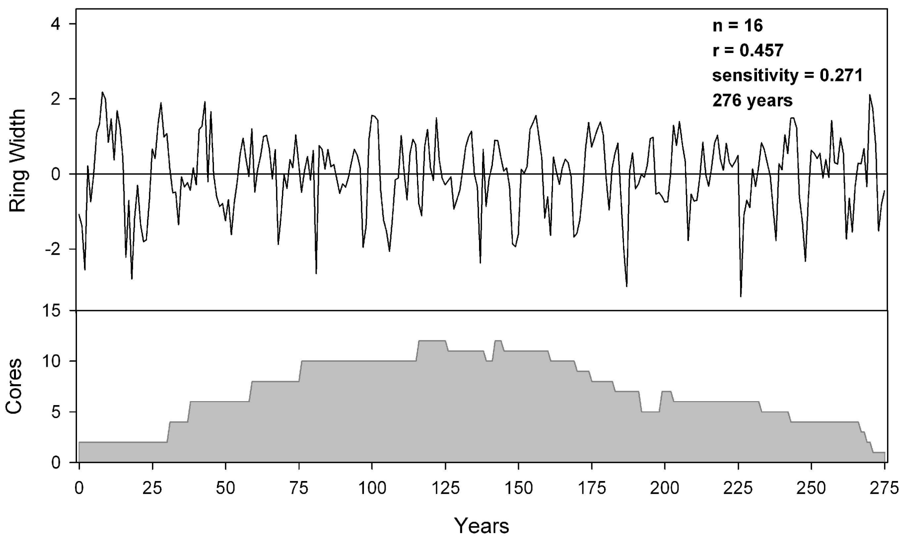

Fig. 8. Tree ring floating chronology from 13 cross-sections collected near the 2010 ice front, covering 276 years, showing high interannual variability.

Discussion Paper | Discussion Paper | Discussion Paper | Discussion Paper |

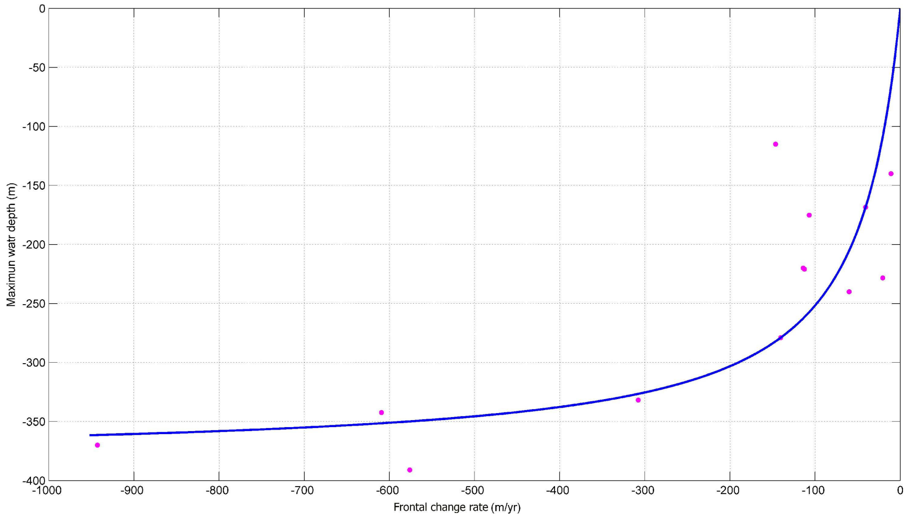

Fig. 9. Relationship between frontal change rates and maximum water depths in Jorge Montt fjord. The blue line indicates a polynomial best fit regression ($r^2 = 0.67$) between frontal change rate and water depth.

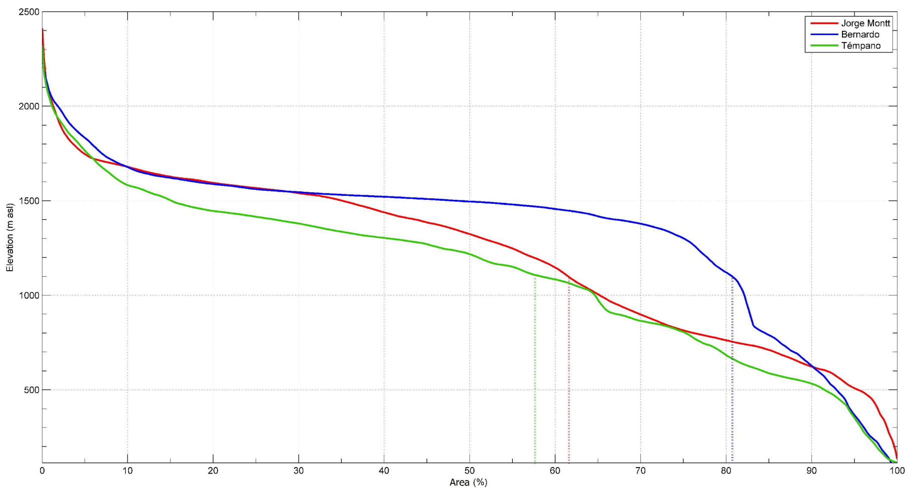

Fig. 10. Hypsometric curves of Glaciares Jorge Montt, Bernardo and Témpano, derived from 2000 AD SRTM digital elevation model. Modern ELA for all three glaciers was estimated at 1100 m asl. The AAR of Bernardo is 0.80, much higher than Jorge Montt (0.61) and Témpano (0.58). The present ELA at Jorge Montt is approaching the main plateau, whilst at Témpano it intersects the main plateau. At Bernardo, the present ELA is still within the steeper lower part of the glacier.

Discussion Paper | Discussion Paper | Discussion Paper | Discussion Paper |